Biomaterials Advances xxx (xxxx) xxx

Contents lists available at ScienceDirect

Biomaterials Advances

journal homepage: www.elsevier.com/locate/bioadv

Injectable recombinant human collagen-derived material with high cell adhesion activity limits adverse remodelling and improves pelvic floor function in pelvic floor dysfunction rats

Hu Li [a], Shuang You [a], Xia Yang [d], Shuaibin Liu [a,*], Lina Hu [a,b,c,**]

[a] Department of Obstetrics and Gynecology, The Second Affiliated Hospital, Chongqing Medical University, Chongqing 400010, China
[b] Joint International Research Lab for Reproduction and Development, Ministry of Education, Chongqing 400010, China
[c] Reproduction and Stem Cell Therapy Research Center of Chongqing, Chongqing 400010, China
[d] Fudan-Jinbo Joint Research Center, Fudan University, Shanghai 200302, China

ARTICLE INFO

Keywords:
Female pelvic floor dysfunction
Recombinant human collagen
Cell adhesion activity
ECM assembly

ABSTRACT

Female pelvic floor dysfunction (FPFD) is a life-changing condition that severely affects women's physical and mental health. Despite the effectiveness of current treatments for FPFD, there is a high rate of short-term recurrence. Here, we introduced an injectable recombinant human collagen (rhCOL)-derived material with high cell adhesion activity to achieve pelvic floor repair and extracellular matrix (ECM) assembly. In our study, rhCOL promoted human uterosacral ligament fibroblast (HULF) adhesion, migration, and collagen I and III expression and regulated the metabolism of HULFs *in vitro*. Subsequently, we established a rat model of FPFD. Then, rhCOL, including rhCOLI and rhCOLIII, was perivaginally injected into FPFD rats, resulting in a significant increase in abdominal urine leak point pressure (LPP) and maximum tensile strength compared to the FPFD model group. Better organization of the lamina propria and muscularis in FPFD rats was observed after 14 days of rhCOL treatment. Meanwhile, the expression of collagen I, collagen III, and TIMP1 was upregulated, and MMP2 was downregulated. Furthermore, rhCOL promoted HULF adhesion, migration, and ECM synthesis by upregulating the focal adhesion kinase (FAK)/RhoA/ROCK signalling pathway *in vitro and in vivo*. These findings suggest that the perivaginal injection of rhCOL is a promising treatment for FPFD with potential for future clinical use.

1. Introduction

Female pelvic floor dysfunction (FPFD) is a group of gynaecologic disorders that often manifest as pelvic floor organ prolapse (POP) and stress urinary incontinence (SUI) [1]. According to previous reports, 11%–35.5% of women suffer from FPFD worldwide [2,3]. Although numerous clinical studies have revealed that age, pregnancy, childbirth, declining oestrogen levels, constipation, and obesity are all causative factors for FPFD [4–6], the pathogenic mechanisms of FPFD have not been fully elucidated. Surgery is the primary treatment for patients with FPFD. Depending on the severity of the disease, patients may undergo urethral suspension, soft tissue repair, or hysterectomy, but nearly 30% of patients will experience recurrence after surgery [7]. In recent years, synthetic biological mesh, as well as collagen urethral bulking agents, have been developed and applied for FPFD patients, which led to improvements in long-term recovery. However, these biomaterials have limitations and pose more challenges due to their side effects, including chronic erosion of the surgical site, persistent pain, and acute allergic reactions [8,9]. There is an urgent need to find new therapies to enhance the repair and regeneration of damaged tissues in FPFD.

The fascia, ligaments, and muscles of the pelvic floor form a complex pelvic floor support system to support the pelvic organs. The extracellular matrix (ECM) is the main component of ligaments, fascia, and the vaginal wall; the ECM is a complex mixture of long-chain proteins, including collagen, elastin, and proteoglycans [10]. It is maintained by fibroblasts through the secretion of proteases and growth factors, which modulate the synthesis and breakdown of structural fibres. Previous studies [11,12] have revealed that the pathogenesis of FPFD is closely related to ECM metabolism and remodelling. The limited endogenous ability to modify the ECM is the critical factor that inhibits repair and regeneration [13]. Collagen, as a major component of the ECM of pelvic floor supporting tissues, maintains the elasticity and toughness of pelvic floor connective tissues [14]. The content of type I and type III collagen was reduced in FPFD. In addition, the matrix metalloproteinases (MMPs) associated with collagen degradation were overexpressed, and the expression levels of tissue inhibitors of metalloproteinases (TIMPs) were downregulated [14,15]. Therefore, maintaining collagen metabolic homeostasis may be a necessary treatment for FPFD.

* Corresponding author.
** Correspondence to: L. Hu, Department of Obstetrics and Gynecology, The Second Affiliated Hospital, Chongqing Medical University, Chongqing 400010, China.
E-mail addresses: 136134949@qq.com (S. Liu), cqhulina@hospital.cqmu.edu.cn (L. Hu).

http://dx.doi.org/10.1016/j.msec.2022.112715
Received 6 September 2021; Received in revised form 13 January 2022; Accepted 9 February 2022
Available online xxxx

Type I collagen and Type III collagen are the major structural components of the ECM of skin, cardiac, and vascular tissues; type I collagen has tensile resistance and supports tissues, and type III collagen maintains the elastic properties of tissues [16]. Type I collagen and Type III collagen bind to collagen receptors and perform multiple biological functions. They not only play a supportive role in cell adhesion, differentiation, and migration [17,18] but also promote ECM synthesis and M2 macrophage polarization as well as angiogenesis and platelet aggregation [19]. Due to its low immunogenicity, good biocompatibility, and biodegradability, collagen has been developed as a biomaterial and is widely used for cartilage regeneration, wound healing, and the repair of damaged tissues and dysfunctional organs in humans [20,21]. However, there are still some problems and more challenges that limit the clinical translation, such as the animal origin, toxicity of chemical cross-linking agents and a challenging problematic and expensive purification process of collagen from animal tissues [22]. Recombinant human collagen (rhCOL) thus represents a desirable alternative because it is safer, potentially less expensive and has higher solubility and absorbability than native collagen [23,24]. A recent study showed that recombinant protein T16 (rhCOLIII), derived from human type III collagen, has a stable triple-helical conformation and exhibits potent cell adhesion. The intravaginal administration of rhCOLIII repaired the vaginal epithelium and promoted ECM assembly [25]. Both human collagen alpha-2 type I-derived peptides and human collagen alpha-1 type I-derived peptides stimulate collagen synthesis, wound healing, and elastin production in normal human dermal fibroblasts [26]. rhCOLI and rhCOLIII have also been shown to be an excellent ECM for damaged corneal and cardiac recovery [19].

Here, instead of using animal-derived collagens, we synthesized injectable recombinant proteins derived from human type I collagen and human type III collagen to provide an effective treatment for FPFD. rhCOL with high cell adhesion ability, the promotion of ECM remodelling and improved pelvic floor function in a model of pelvic floor dysfunction rats. In an *in vitro* study, we observed functional improvement in response to rhCOL treatment in human uterosacral ligament fibroblasts (HULFs), possibly by promoting cell adhesion, migration, and ECM synthesis by activating the focal adhesion kinase (FAK)/RhoA/ROCK signalling pathway.

2. Materials and methods

2.1. Preparation of the rhCOL

rhCOLI was derived from the Gly932-Ser991 fragment of human type I collagen α1 chains, and rhCOLIII was derived from the Gly483-Pro512 fragment of human type III collagen α1 chains. Clinical-grade rhCOL was acquired from Shanxi Jinbo Bio-Pharmaceutical CO., Ltd., and it was produced in a laboratory under good manufacturing practice (GMP) of medical products conditions. Briefly, the preparation of rhCOLI and rhCOLIII was performed as follows. rhCOLI consists of 4 tandem repeats of the triple-helix fragment of hCOL1α1, Gly932-Ser991. rhCOLIII consists of 16 tandem repeats of the triple-helix fragment of hCOLIIIα3, Gly483-Pro512. Recombinant expression vectors containing rhCOLI and rhCOLIII genes were transformed into competent *E. coli* (BL21 (DE3)). After induction with isopropylthio-β-galactoside, the expressed proteins were purified with nickel-chelate chromatography and anion-exchange chromatography.

2.2. Patient selection, tissue processing, and cell culture

The retrieval of biopsies from patients was reviewed and approved by the Ethics Committee of The Second Affiliated Hospital of Chongqing Medical University. All patients provided written informed consent. Patients were eligible for inclusion in the FPFD group if they had evidence of severe pelvic organ prolapse (POP-Q stage III-IV) with stress urinary incontinence. Exclusion criteria included a history of connective tissue disease, endometriosis, acute or chronic pelvic inflammatory disease, malignant tumour, pelvic surgery, chronic debilitating disease, and oral oestrogen within 3 months. Surgical specimens of approximately 0.5 cm were taken from the uterosacral ligament. Freshly isolated tissues were immediately placed in Dulbecco's modified Eagle's medium (DMEM, Gibco, UK) containing 15% fetal bovine serum (FBS, PAN, Germany). Within 2 h, cells were isolated and cultured as described previously [27]. Cells were grown in DMEM supplemented with 15% FBS and 1% streptomycin/penicillin solution and incubated at 37 ˚C, 95% humidity, and 5% CO_2. All experiments were performed with fibroblasts from early passages (3–5).

2.3. Cell adhesion

Before cell culture, lyophilized rhCOLI, rhCOLIII and hydrolysate of bovine collagen I (bvCOLI, Solarbio, China) were diluted with PBS to the predetermined concentrations (25 μg/ml), used to coat 96-well culture plates and allowed to incubate in an incubator at 37 ˚C for 2 h. Then, the solution was gently removed, plates were blocked with 5% bovine serum albumin (BSA) in an incubator at 37 ˚C for 1 h. HULFs (1×10^5 cells/well) were added to the well and incubated for 1 h at 37 ˚C, followed by washing four times with PBS. Relative cell adhesion rates were measured by using a Cell Counting Kit (CCK-8, MCE, US) on a microplate reader (Thermo Scientific™ Varioskan™ LUX, US). For inhibitor experiments, cells were plated on substrates of interest in the presence of one of the following reagents: PF573228 (20 mM, MCE, US) and C3 transferase protein (3 μg/ml, Cytoskeleton, US). Inhibitors remained in the media during the experiment.

2.4. Cytotoxicity assay

HULFs were seeded into a 96-well culture plate (3×10^3 cells/well). Lyophilized rhCOLI, rhCOLIII, and bvCOLI were dissolved in DMEM, and each solution was added to a cell suspension at a final concentration of 5 mg/ml. Cell viability was measured and analysed after 48 h by using a Cell Counting Kit-8.

2.5. Scratch assay

HULFs (5×10^5 cells/well) were seeded into coated 6-well plates overnight, completely covered the culture plate. A perpendicular scratch was made in the cells on the culture plate using a 1000 μl pipette tip, and the scratched cells were removed with 3 washes with PBS. Medium containing 0.2% FBS was added. Cells were photographed at 0 and 24 h by an inverted microscope (Nikon Eclipse Ts2F, Japan).

2.6. Scanning electron microscopy (SEM)

For SEM, cells (1×10^5/well) were cultured in a coated 6-well plate for 12 h. After washing three times with PBS, the electron microscope solution was fixed at room temperature for 2 h and stored at 4 ˚C, and then ethanol gradient dehydration was performed to prevent cell deformation. The critical point drying method was used to dry the sample for 2 h. After gold plating and vacuum coating, cells were observed by SEM (Hitachi, S-3000 N, Japan).

2.7. Western blot assay

Cells were lysed in RIPA buffer (Beyotime, China) with 1% protease and 1% phosphatase inhibitors (Beyotime, China). The total protein concentration in cell supernatants was measured by a bicinchoninic acid (BCA) protein assay kit (Beyotime, China), then equal amounts of proteins were separated with 10% sodium dodecyl sulfate-polyacrylamide gel electrophoresis (SDS-PAGE). Proteins were transferred onto 0.45-mm PVDF membranes (Millipore, US), and membranes were blocked with 5% BSA solution for 1.5 h at room temperature. Membranes were incubated with a primary rabbit anti-Collagen I (1:1000, ab260043, Abcam, US), anti-Collagen III (1:1000, ab184993, Abcam, US), anti-Vinculin (1:1000, ab129002, Abcam, US), anti-FAK (1:1000, CST, US), anti-phosphorylated FAK (pFAK (Tyr397), 1:1000, CST, US), anti-pFAK (Try576/577) (1:1000, CST, US), anti-FAK (Try925) (1:1000, CST, US), anti-RhoA (1:500, ab187027, Abcam, US), and anti-ROCK (1:1000, ab45171, Abcam, US) antibodies at 4 ˚C, overnight with GAPDH (1: 4000, 0494–1-

AP, Proteintech, China) as the loading control. Membranes were incubated with a secondary goat anti-rabbit IgG antibody (bs-40295G-HRP, Bioss, China) for 0.5 h at room temperature. Finally, the membrane signals were visualized by enhanced chemiluminescence (BeyoECL, Beyotime, China) and exposed with a ChemiDoc XRS system (Bio-Rad, US). The image data were analysed by NIH ImageJ software (version 1.53a).

2.8. Immunofluorescence and confocal microscopy observation

After 12 h of culture, cells were washed three times with PBS before being fixed with 4% paraformaldehyde at room temperature for 10 min, permeabilized with 0.1% Triton X-100 in PBS for 10 min, blocked with 5% BSA at room temperature for 1 h, and incubated with the primary antibodies anti-vinculin (1:200, ab129002, Abcam, US) and anti-phalloidin (1:200, G104, Servicebio, China) overnight at 4 °C. The secondary antibody was added and incubated at 4 °C for 1 h in darknass. Nucleic acid staining was also performed by adding DAPI solution (Beyotime, China) for 5 min in darkness. Cells were observed by confocal laser scanning microscopy (Nikon Eclipse Ti, Japan).

2.9. Co-immunoprecipitation

A total of 50 μl Protein A/G magnetic beads were added to 400 μl pFAK (Tyr397) (1:50) antibody solution and were rotated for 30 min at room temperature. The sample containing the antigen beads was collected against the side of the tube on magnetic-activated cell sorting (MACS) Separators (Miltenyi, Germany). Then, cell supernatant containing an anti-vinculin (1:50) antibody was added and incubated with rotation for 30 min at room temperature, allowing vinculin to bind to the Protein A/G magnetic beads-pFAK (Tyr397) complex. The beads were separated and mixed with loading buffer. After being heated at 95 °C for 5 min, the beads were separated again, and the final supernatant was analysed with SDS-PAGE.

2.10. RhoA activation assay

Rho activation was measured using an Active Rho detection kit (Cytoskeleton, US) following the manufacturer's instructions. Briefly, equal amounts of protein from lysates (500 μg total cell protein) were incubated with rhotekin-RBD beads at 4 °C for 1 h on a rocker. The rhotekin-RBD beads were pellet by MACS separators. After the supernatant was removed, the magnetic beads were washed with wash buffer twice. A total of 10 μl of 5× loading buffer (Beyotime, China) was added, the bead sample was boiled for 5 min. Finally, the samples were separated by SDS-PAGE and detected by western blot analysis using a specific anti-RhoA antibody.

2.11. Metabolite extraction and analysis

Cells (1×10^6/dish) were cultured in a coated 10 cm dish that contained a complete medium (DMEM supplemented with 15% FBS, 1% streptomycin/penicillin) for 72 h, and 1 ml of cell culture was taken from each culture dish. After the medium was centrifuged at 13000 rpm at 4 °C for 15 min, the supernatants were isolated, and 20 μl of internal standard (2,3,3,3-d4-alanine, 10 mM, Thermo, US) was added. The blank control medium for each experimental group was treated the same way without any cell components. Isolated supernatants were concentrated by using a SpeedVac (Labconco B, US) for 4 h followed by resuspension in 200 ml of sodium hydroxide (1 M) and methyl chloroformate (MCF) derivatization based on a previous protocol [28]. The derivatives of the MCF metabolites were analysed using a GC7890B system (Agilent, US) coupled to an MSDD5977A mass spectrometer (Agilent, US) with an electron beam energy of 70 eV. A ZB-1701 GC capillary column was used to incorporate the gas chromatography (GC) column incorporated in the GC oven was an A30 m × 250 μm id ×0.15 mm with 5 m guard column, Phenomenex), and the GC oven settings and mass spectrometry parameters were implemented according to Smart et al. [28]. The Automated Mass Spectral Deconvolution and Identification System (AMDIS) achieved chromatogram deconvolution and compound identification in conjunction with an in-house MCF-derivatised mass spectrum library and commercially available National Institute of Standards and Technology (NIST) mass spectrum library (http://www.nist.gov/srd/nist1a.cfm) [29]. The relative abundances of identified metabolites were extracted using an automated an XCMS-R script. Principal component analysis (PCA), heat maps, and metabolic pathway analysis were performed on the website MetaboAnalyst5.0 (https://www.metaboanalyst.ca/) [30].

2.12. Animal experiments

2.12.1. FPFD model establishment

All animal studies were approved by the Ethics Committee of Chongqing Medical University. Sixty-five female Sprague-Dawley rats (2 months old) with an average weight of 220–260 g were provided by the Experimental Animal Center of Chongqing Medical University. Rats were fed and received tap water in an environment with a temperature of 22 ± 2 °C, humidity of 50–60%, and a 12-h light/dark cycle. The rats were anaesthetized by intraperitoneal injection of urethane (1.2 g/kg), and bilateral ovaries were excised. Then, the bladder was emptied by catheterization, the F12 catheter with the tip removed was inserted into the vagina of rats (2–3 cm). After the balloon was filled with 3 ml of saline, the rat was placed in a supine position on the edge of a table, and the foley catheter was allowed to hang with 0.15 kg weight attached to its free-hanging end. After 4 h, the catheter was removed, followed by the administration of 80,000 U penicillin sodium by a single intramuscular injection. To be characterized as having multiple birth injuries, rats were subjected to vaginal balloon dilatation once again after 2 weeks. Then, the presence of FPFD was confirmed after 4 weeks by urodynamic tests and biomechanical tests.

2.12.2. Perivaginal injection and urodynamic test

The control group received a sham operation. After establishing the FPFD rat model, the PBS (0.01 M), rhCOLI (5 mg/ml), rhCOLIII (5 mg/ml), and bvCOLI (5 mg/ml) were prepared, a total of 200 μl of solution (PBS, rhCOLI, rhCOLIII, and bvCOLI) was injected into the entire vaginal mucosal layer from the vaginal opening to the cervix under direct visualization in the four directions (the three o'clock, six o'clock, nine o'clock, and twelve o'clock directions). Two weeks after the injection, urodynamic function was evaluated by measuring the maximum bladder volume (MBV) and leak point pressure (LPP) according to a previously reported method [31]. Briefly, 2 days before the test, a PE-50 catheter was inserted into the bladder of FPFD rats. The rats were anaesthetized by the intraperitoneal injection of urethane (1.2 g/kg). After the bladder was emptied, a manometry catheter was connected to a pressure transducer (YPJ01, Chengdu Instrument Factory, China). The perfusion tube was connected to a microinjection pump, which continuously injected saline into the bladder (12 ml/h), and during this process, the waveform graph was recorded. When the bladder volume reached half of the total volume, the rat's abdomen was gently pressed with one finger to increase the bladder pressure until the first drop of saline appeared at the urethral opening. At this point, the finger was quickly removed, and the peak pressure was recorded. The bladder was emptied and refilled, and the procedure was repeated three times in each rat.

2.12.3. Biomechanical testing

After sacrifice, the vaginal soft tissues were carefully separated and continually moistened with 0.9% sodium chloride and manipulated over an ice bath to prevent tissue breakdown. The distal 5 mm of the vagina and cervix was placed inside a tissue clamp along the longitudinal axis. Specimens were preloaded to 0.1 N, followed by 10 cycles of preconditioning at a distension rate of 10 mm/min between 0 and 2 mm by and ElectroForce 5500 (Bose, Germany). Then, under the same parameters, the vaginal tissue was uniaxially stretched to rupture, and the force at maximum loading (N) and distension distance of the fracture were recorded.

2.12.4. Immunohistochemistry

After measuring the MBV and LPP, the entire length of the vagina was removed from the rats. Tissues were fixed in 4% paraformaldehyde, embedded in paraffin, and cut into 0.5-μm thick sections along the transverse axis. For histological observation, haematoxylin–eosin (HE) and masson's trichrome (MT) staining were carried out [25]. For immunohistochemistry, the paraffin sections were dried at 60 ˚C for 2 h and further deparaffinized by xylene. After dehydration with gradient alcohol, the sections were kept in boiling water for 15 min for antigen retrieval, followed by incubation with 3% H_2O_2 at 37 ˚C for 10 min. Sections were blocked with 5% goat serum at 37 ˚C for another 15 min. Primary anti-Collagen I (1:300, 14,695–1-AP, Proteintech, China), anti-Collagen III (1:250, 22,734–1-AP, Proteintech, China), anti-MMP2 (1:250, 10,373–2-AP, Proteintech, China), anti-TIMP1 (1:250, 16,644–1-AP, Proteintech, China), anti-pFAK (Tyr397) (1:200, bs-3159R, Bioss, China), and anti-ROCK (1:250, ab45171, Abcam, US) antibodies were added to the sections and incubated at 4 ˚C overnight. After rewarming, the sections were stained with the secondary antibody at 37 ˚C ˚C for 15 min. Finally, 3,3′-diaminobenzidine (DAB) staining was performed, at least three random fields of view were selected from each slice to be photographed, and the images were acquired by a Nikon instrument and analysed by ImageJ software.

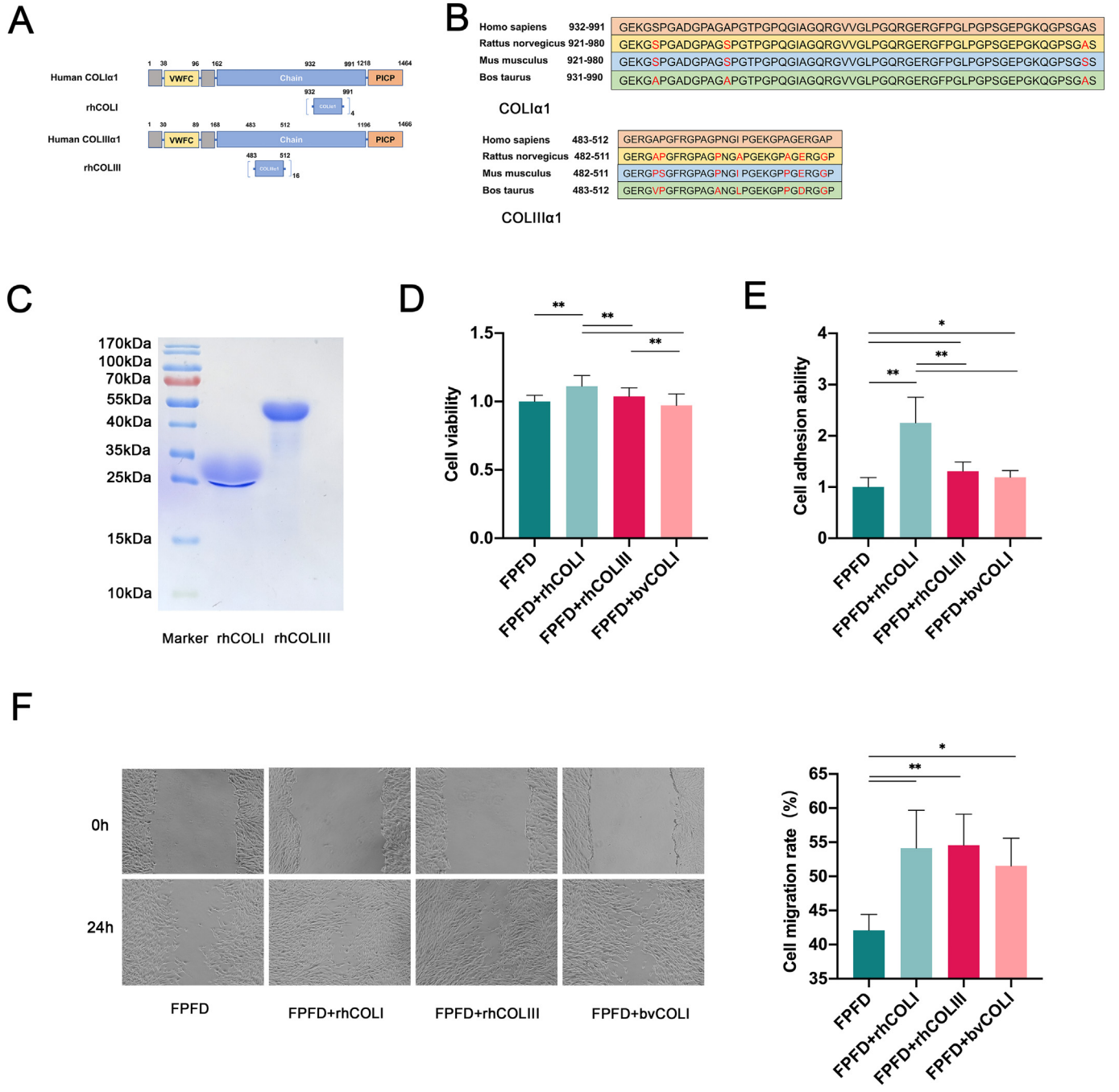

Fig. 1. rhCOL has specific repeating structures with excellent biological functions. (A) The localization and composition of rhCOL. (B) Sequence homology alignment of the hCOL1α1 932–991 segment and hCOL3α1 483–512 segment from *Homo sapiens*, *Rattus norvegicus*, *Mus musculus*, and *Bos taurus*. (C) The molecular weight of rhCOL. (D) Cell cytotoxicity was detected by a CCK-8 assay after 48 h of treatment with rhCOLI, rhCOLIII, and bvCOLI at 5 mg/ml. (E) The cell adhesion ability was detected by a cell adhesion assay after coating with rhCOLI, rhCOLIII, and bvCOLI at 25 μg/ml. (F) The cell migration ability was measured by scratch assay after 24 h of treatment with rhCOLI, rhCOLIII, and bvCOLI at 25 μg/ml (*$P < 0.05$, **$P < 0.01$).

2.12.5. Quantitative RT-PCR analysis

Total RNA from vaginal tissues was isolated by using TRIzol reagent (Ambion, US), and 1 μg RNA was used for a reverse transcription reaction with PrimeScript RT Master Mix (Takara, Japan) to create complementary DNA (cDNA) following the manufacturer's instructions. The fluorescence quantification of polymerase chain reactions was performed with SYBR Premix Ex Taq II (Takara). The reaction conditions were 95 °C for 30 s, 95 °C for 5 s, and 60 °C for 30 s, which were repeated for 40 cycles. The tissues were from three independent experiments, and GAPDH was used as a housekeeping gene to normalize the gene expression. The relative quantification was performed to calculate the $2^{-\triangle\triangle CT}$ value. The primers are listed in Table S1.

2.13. Statistical analysis

The experimental data in each group were from at least three different patients or rats. Each patient or rat was considered as one repetition. GraphPad Prism 8.4.0 (GraphPad Software Inc., US) software was used for data analysis. All experimental values were presented as the mean ± standard deviation. One-way analysis of variance (ANOVA) followed by Tukey's multiple comparisons test was used. A significant difference was defined as $P < 0.05$. ($^{*}P < 0.05$, $^{**}P < 0.01$).

3. Results

3.1. rhCOL has a specific repeating structure with excellent biological function

hCOLIα1 is composed of 1464 amino acids, and hCOLIIIα1 is composed of 1466 amino acids. However, the structures and functions of the hCOL1α1 932–991 segment and hCOL3α1 483–512 segment have not yet been elucidated, so in previous studies, we resolved their core crystal structures and deposited them in the Protein Data Bank (PDB entries: 6A0A, 6A0C, and 7CWk). Furthermore, we synthesized rhCOLI which consists of 4 tandem repeats of hCOL1α1 932–991 segment and rhCOLIII which consists of 16 tandem repeats of hCOL3α1 483–512 segment (Fig. 1A); both rhCOLI and rhCOLIII (rhCOL) have a triple-helix structure composed of a leading strand, a middle strand, and a trailing strand. rhCOLI had Gly-Glu-Arg, Gly-Phe-Pro, and Gly-Lys-Glu triple-helix peptide structures, and rhCOLIII had Gly-Lys-Glu and Gly-Glu-Arg triple-helix peptide structures. These small triple-helix peptide structures had relatively high adhesion and biological activity in previous studies [32]. Thus, the tandem repeated rhCOLI and rhCOLIII proteins may bind to many cell membrane proteins. In SDS-PAGE, rhCOLI was approximately 25 kDa, and rhCOLIII was approximately 50 kDa (Fig. 1C). Both rhCOLI and rhCOLIII had a high purity level.

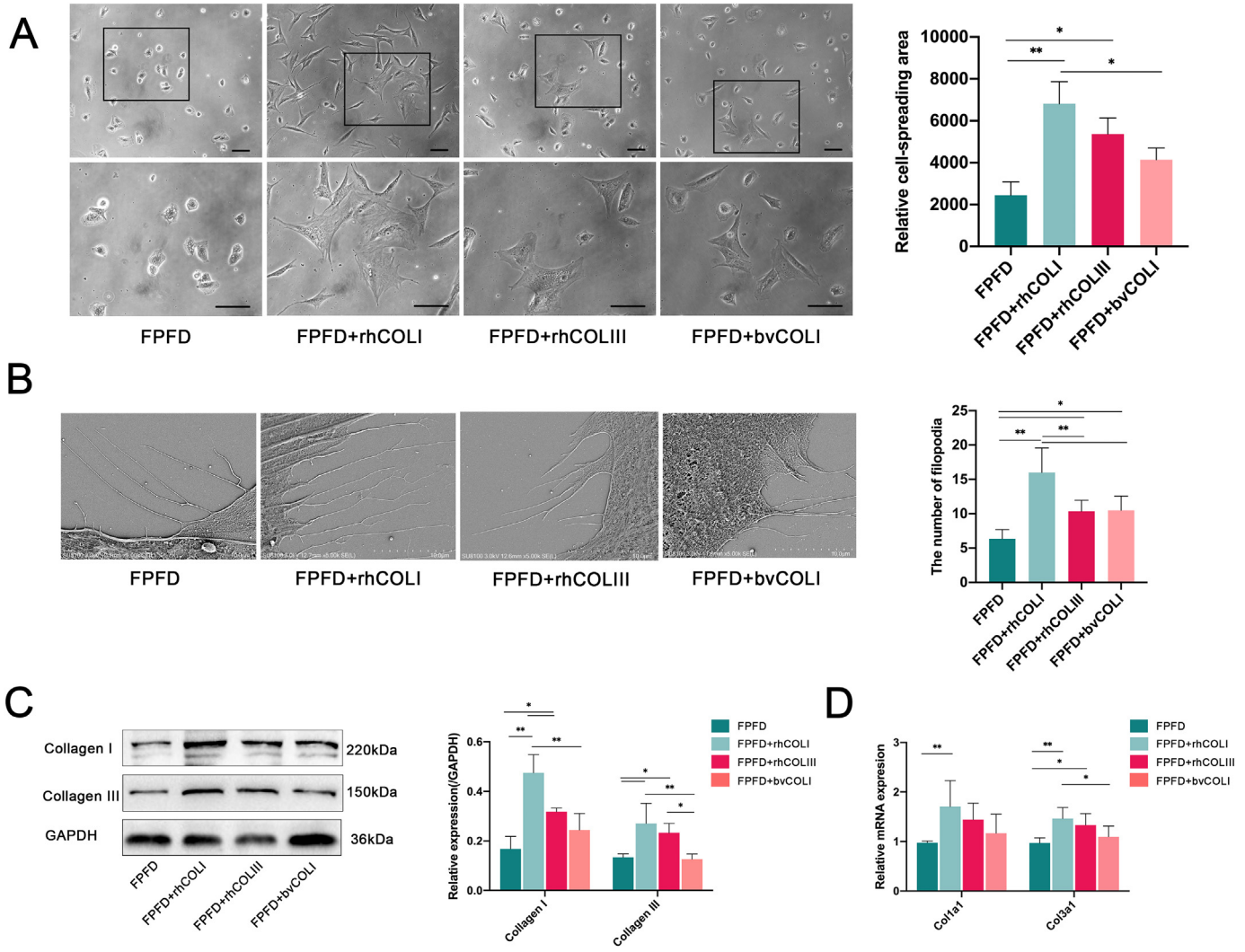

Fig. 2. rhCOL increases cell-spreading area and stimulates collagen synthesis *in vitro*. (A) Morphological observation and cell-spreading area under a light microscope after 12 h of treatment with rhCOLI, rhCOLIII, and bvCOLI (scale bar = 100 μm). (B) The distribution of rhCOL and filopodia was examined by SEM after 12 h of treatment with rhCOLI, rhCOLIII, and bvCOLI (scale bar = 10 μm). (C) The expression of collagen I and III was detected by western blotting after 72 h of treatment with rhCOLI, rhCOLIII, and bvCOLI. (D) The relative mRNA expression of Collagen I and Collagen III was detected by RT-PCR after 72 h of treatment with rhCOLI, rhCOLIII, and bvCOLI ($^{*}P < 0.05$, $^{**}P < 0.01$).

Nontoxicity is an important parameter to examine when determining whether biomaterials can be used in humans. To determine the cytotoxicity of rhCOL and animal collagen, HULFs were successfully isolated from six patients with severe pelvic floor dysfunction (Fig. S1C), and we performed a CCK-8 assay. No significant cytotoxicity was found for rhCOL at concentrations as high as 5 mg/ml. Surprisingly, the rhCOLI group, not the bvCOLI group, had a weak cell proliferation-promoting effect compared to the FPFD and bvCOLI groups (Fig. 1D). Cell adhesion activity is an important biological function of collagen proteins. bvCOLI is a soluble hydrolysate of bovine collagen I, which can be dissolved in a 10 mg/ml aqueous solution at most (Fig. S1A, S1B). Hydrolysate of bovine collagen I contains many bioactive peptides and is easily soluble in water. These hydrolysate peptides have been shown to have the same cell-adhesive activity as full-length bovine collagen I [33]. An adhesion assay showed cell adhesion was higher in the rhCOL group than the FPFD group, and rhCOLI had the most potent effect. The rhCOLIII and bvCOLI groups showed similar cell adhesion abilities (Fig. 1E). Compared with cells treated with 0.2% FBS, the migration ability of HULFs treated with rhCOL was significantly enhanced (Fig. 1F). In addition, rhCOL also promoted adhesion, migration, and extracellular matrix synthesis of wild-type HULFs isolated from non-FPFD donors (Fig. S1GI). Thus, rhCOL, which has significant collagen properties, is expected to be safe for use as a collagen-derived biomaterial in clinical applications.

To verify the function of rhCOL, an ideal animal model is needed, which requires a high degree of homology between rhCOL and animal collagen. The ideal animal model could be used to reduce immunogenicity and exert biological effects. When we compared the corresponding amino acid sequence of the rhCOL proteins among humans and other mammals, we found that hCOL1α1 932–991 segment was 98.3% homologous with rat and *Bos taurus*, which was higher than mouse (96.7%). hCOL3α1 483–512 segment was 93.3% homologous to that of the rat, which was higher than that of the mouse (86.7%) and *Bos taurus* (80%), so the rat was an ideal animal model (Fig. 1B).

3.2. rhCOL increased cell-spreading area and stimulated collagen synthesis in vitro

After HULFs were treated with rhCOLI, rhCOLIII, and bvCOLI for 12 h, the cell-spreading area of all treatment groups showed a significant increase, among which the rhCOLI group showed the most marked increase compared with the FPFD group, while the rhCOLIII and bvCOLI groups showed similar cell-spreading areas (Fig. 2A). The local distribution of rhCOL and the filopodia distribution in HULFs were further examined by SEM. Collagen was evenly distributed over the culture dish and appeared finely granular. The distribution of fibroblast pseudopods was dense and increased in the rhCOLI group compared to the FPFD group, while the number of fibroblast pseudopods was also greater in the rhCOLI group than in the rhCOLIII and bvCOLI groups (Fig. 2B). Although the number of fibroblast pseudopods in the rhCOLIII group increased compared to that in the FPFD group, the number of fibroblast pseudopods was similar to that in the bvCOLI group. To assess the effect of rhCOL on ECM metabolism, we performed western blot assays and RT-PCR. The results showed that rhCOL promoted collagen I and collagen III expression in HULFs, while collagen I expression was more significantly different in the rhCOLI group than in the rhCOLIII group (Fig. 2C, D). In addition, RT-PCR results also suggested that rhCOL increased the expression of MMP2 and TIMP1, but there was no statistical difference (Fig. S1E).

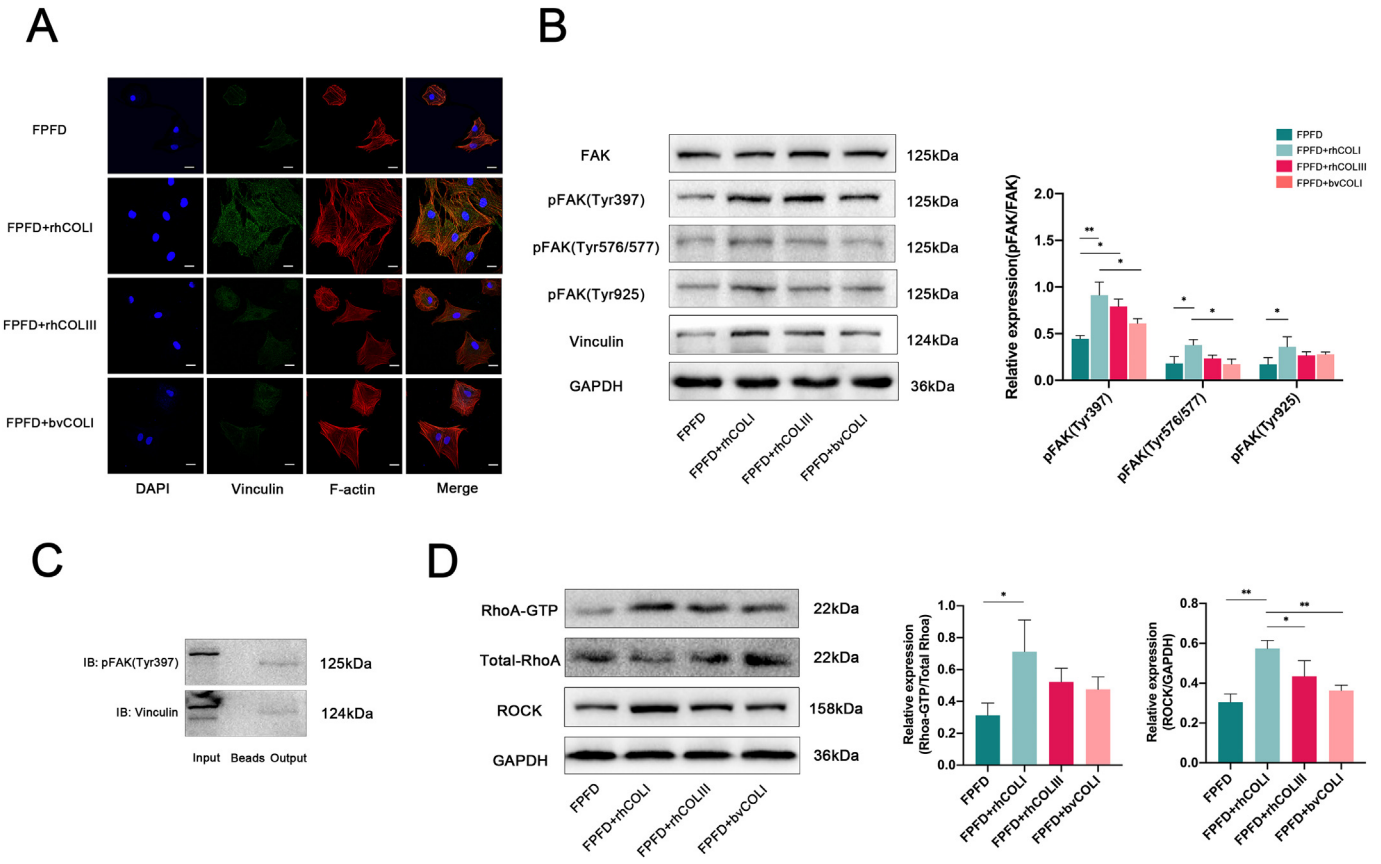

Fig. 3. rhCOL promotes focal adhesion formation and activates the RhoA/ROCK signalling pathway. (A) Representative immunofluorescence images for vinculin and F-actin staining in HULFs after culture with rhCOLI, rhCOLIII, and bvCOLI for 12 h (scale bar = 20 μm). (B) The expression of FAK, pFAK (Tyr397), pFAK (Tyr576/577), pFAK (Tyr925), and vinculin in HULFs after 12 h of culture with rhCOLI, rhCOLIII, and bvCOLI. (C) pFAK (Tyr397) and vinculin interaction in HULFs was determined by co-immunoprecipitation after 12 h of culture with rhCOLI. (D) The expression of ROCK and RhoA-GTP in HULFs after 12 h of culture with rhCOLI, rhCOLIII, and bvCOLI (*$P < 0.05$, **$P < 0.01$).

3.3. rhCOL promotes focal adhesion formation and activates the RhoA/ROCK signalling pathway

Cell adhesion is closely associated with focal adhesion structure formation. Vinculin is a crucial local adhesion protein. To investigate whether rhCOL promoted adhesion plaque formation, we performed immunofluorescence staining for F-actin and vinculin. Vinculin was mainly distributed around the cytoskeleton, and the vinculin and extension range of F-actin were significantly increased after treatment with rhCOL (Fig. 3A). Vinculin binds to pFAK to form adhesion plaques that mediate cell adhesion. We further analysed the phosphorylation of FAK at different phosphorylation sites. Significant FAK phosphorylation at Tyr397 was observed after treatment with rhCOL (Fig. 3B). To clarify the direct interaction between pFAK (Tyr397)and vinculin, co-immunoprecipitation experiments were performed and suggested that FAK and vinculin directly interact (Fig. 3C), FAK at Tyr397, which is the structural protein in the molecular clutch and can only be activated at Tyr397 under contraction, reflecting the intracellular tension as well as the activation of mechanotransduction [34]. Thus, we investigated the classical RhoA/ROCK signalling pathway that mediates intracellular mechanotransduction. Both RhoA-GTP and ROCK were significantly upregulated after treatment with rhCOL (Fig. 3D).

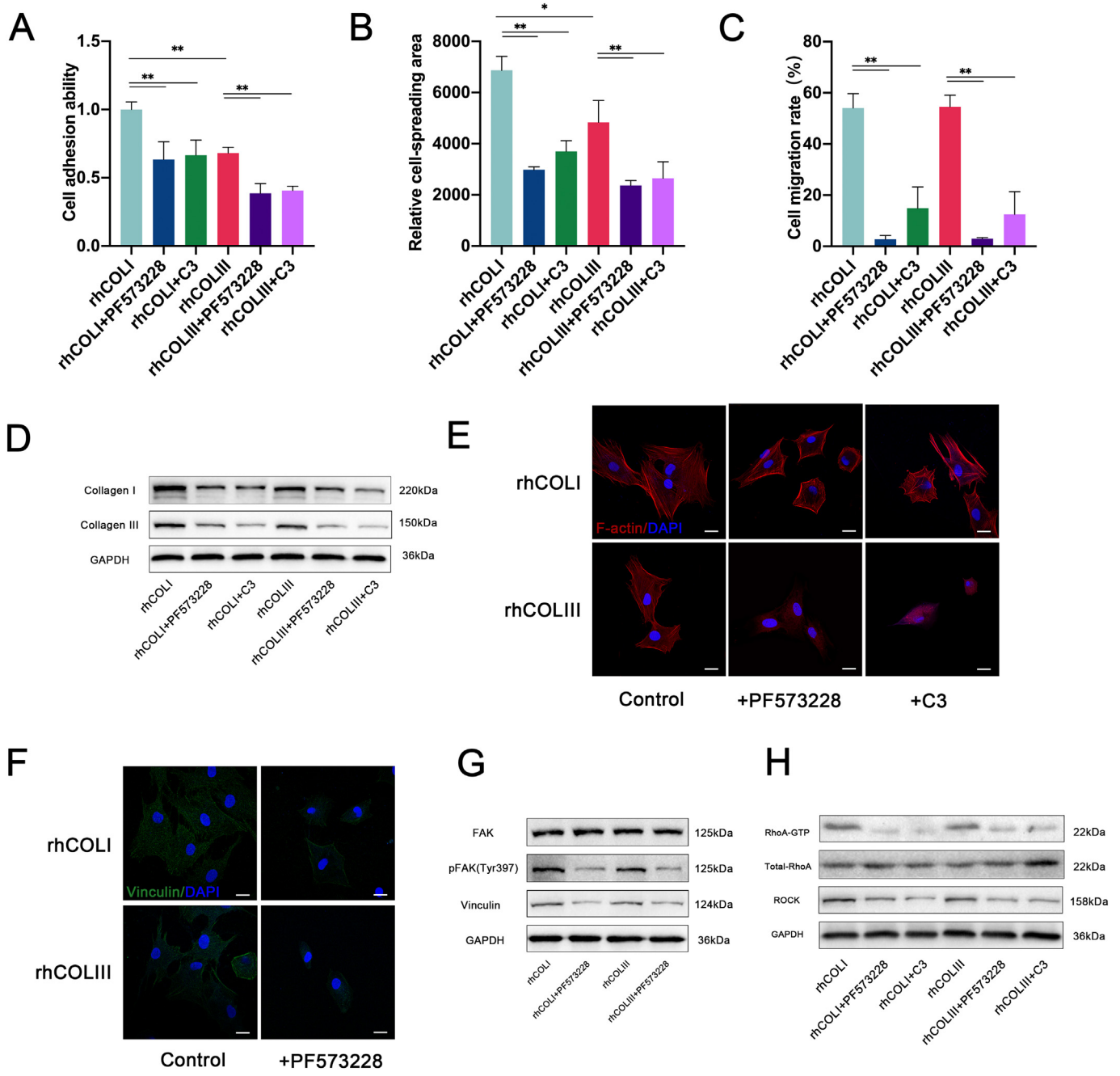

Fig. 4. Inhibition of the expression of pFAK (Tyr397) and RhoA-GTP attenuated cell adhesion and migration. (A) Cell adhesion ability, (B) spreading area, and (C) cell migration rate for PF573228 and C3 treatment after culture with rhCOLI or rhCOLIII. (D) The expression of collagen I and III in HULFs for PF573228 and C3 treatment after culture with rhCOLI and rhCOLIII for 72 h. (E) Representative images of F-actin staining for PF573228 and C3 treatment after culture with rhCOLI and rhCOLIII for 12 h (scale bar = 20 μm). (F) Representative immunofluorescence images for vinculin staining in HULFs for PF573228 treatment after culture with rhCOLI or rhCOLIII for 12 h (scale bar = 20 μm). (G) The expression of FAK, pFAK (Tyr397), vinculin, RhoA-GTP, or ROCK in PF57322 cells treated after 12 h of culture with rhCOLI or rhCOLIII. (H) The expression of RhoA-GTP and ROCK for C3 treatment after 12 h of culture with rhCOLI and rhCOLIII. (*$P < 0.05$, **$P < 0.01$).

3.4. Inhibition of the expression of pFAK (Tyr397), RhoA-GTP attenuated cell adhesion and migration

When HULFs were treated with rhCOL and a pFAK (Tyr397) inhibitor (PF573228) for 12 h, a significant decrease in the cell adhesion capacity (Fig. 4A), cell-spreading area (Fig. 4B), cell migration rate (Fig. 4C) and expression of collagen I and III (Fig. 4D) was observed. Decreases in the cell adhesion capacity (Fig. 4A), cell-spreading area (Fig. 4B), cell migration rate (Fig. 4C), and expression of collagen I and III (Fig. 4D) were also observed in all groups treated with a RhoA-GTP inhibitor (C3 transferase). In addition, PF573228 suppressed the formation of stress fibre (Fig. 4E), expression of vinculin (Fig. 4F, G), RhoA-GTP (Fig. 4H), and ROCK (Fig. 4H), while C3 transferase downregulated the expression of RhoA-GTP and ROCK (Fig. 4H).

3.5. rhCOL modulates uterosacral ligament fibroblast metabolism

After HULFs were treated with rhCOLI or rhCOLIII for 72 h, metabolite profiles in the culture medium were detected. The PCA score plot (Fig. 5A) of the culture medium metabolite profiles revealed a clear separation between the rhCOLI group and FPFD group, as well as a distinct disparity between the rhCOLIII group and the FPFD group. To exclude the effect of rhCOL coating in the medium on metabolite production, we also analysed metabolites in the control medium without HULFs. The results showed no

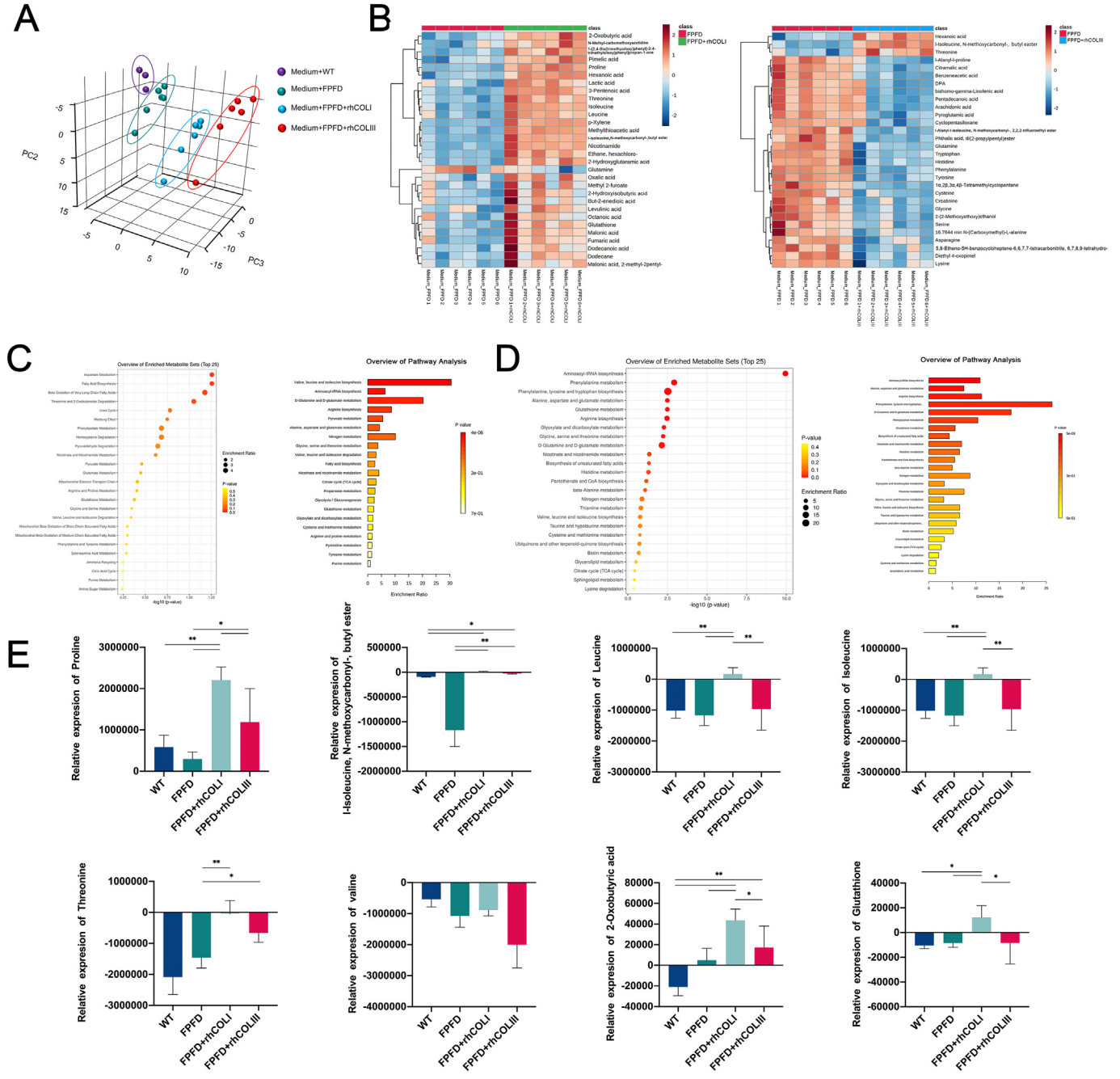

Fig. 5. rhCOL modulates uterosacral ligament fibroblast metabolism after 72 h of treatment. (A) The PCA score plot of the culture medium metabolite profiles. (B) The heatmap of the differential metabolites. (C) Enrichment analysis and KEGG pathway analysis of differential metabolites between the FPFD and rhCOLI groups. (D) Enrichment analysis and KEGG pathway analysis of differential metabolites between the FPFD group and rhCOLIII group. (E) Relative expression of proline, branched-chain amino acids (BCAAs), and antioxidants in all groups (*$P < 0.05$, **$P < 0.01$).

differences in metabolites in the control medium (Fig. S1F). A total of 130 metabolites were detected in all groups. Twenty-nine of the extracellular metabolites, including amino acids, antioxidants, saturated fatty acids, and tricarboxylic acid (TCA) cycle intermediates, were significantly different between the rhCOLI and FPFD groups (Fig. 5B). Increased secretion of metabolites, including four amino acids, one antioxidant, three saturated fatty acids, and three TCA cycle intermediates, was observed in the medium treated with rhCOLI. In the rhCOLI group, the secretion of proline, threonine, leucine, isoleucine, and 2-oxybutyrate was significantly increased, and the absorption of valine tended to decrease compared with that in the FPFD group (Fig. 5E). On the other hand, 54 of the extracellular metabolites were significantly different between the rhCOLIII and FPFD groups (Fig. 5B). Significantly increased secretion of proline and threonine was also observed in the medium treated with rhCOLIII (Fig. 5E). However, most significant extracellular metabolites were absorbed from the culture medium rather than secreted when HULFs were treated with rhCOLIII (Fig. 5B). Differential metabolites were subjected to enrichment analysis and Kyoto Encyclopedia of Genes and Genomes (KEGG) pathway analysis. The arginine and proline metabolism pathway, glutathione metabolism pathway, and valine, leucine and isoleucine biosynthesis pathways were upregulated compared with those of the rhCOLI and FPFD groups (Fig. 5C). At the same time, the valine, leucine and isoleucine biosynthesis pathways were also upregulated compared with those of the rhCOLIII and FPFD groups (Fig. 5D). In addition, we also cultured WT HULFs isolated from 3 non-FPFD donors. rhCOL treated HULFs from FPFD patients were better metabolized than WT HULFs, especially rhCOLI. We observed increased secretion of metabolites such as proline, i-isoleucine, threonine, and 2-oxobutyric acid in the rhCOL group.

3.6. rhCOL improved the histological features of FPFD rats

To assess the therapeutic potential of rhCOL, we randomized FPFD rats to receive a perivaginal injection of PBS, rhCOLI, rhCOLIII, and bvCOLI. Fourteen days after treatment, urodynamic examinations were conducted. For urodynamic examinations, the MBV and LPP were critical indicators for evaluating the prevalence pelvic floor dysfunction in women, and both the MBV and LPP mean values decreased in the model group compared to the control group (Fig. 6B, C), indicating the successful generation of the animal model. The rats in the rhCOL group showed significantly higher values than those in the FPFD group. In contrast, no significant differences were detected between the rhCOL and control groups, thus demonstrating that urethral sphincter continence was restored following rhCOL injection. On the other hand, although the mean MBV and LPP values of the bvCOLI group were elevated compared with those of the

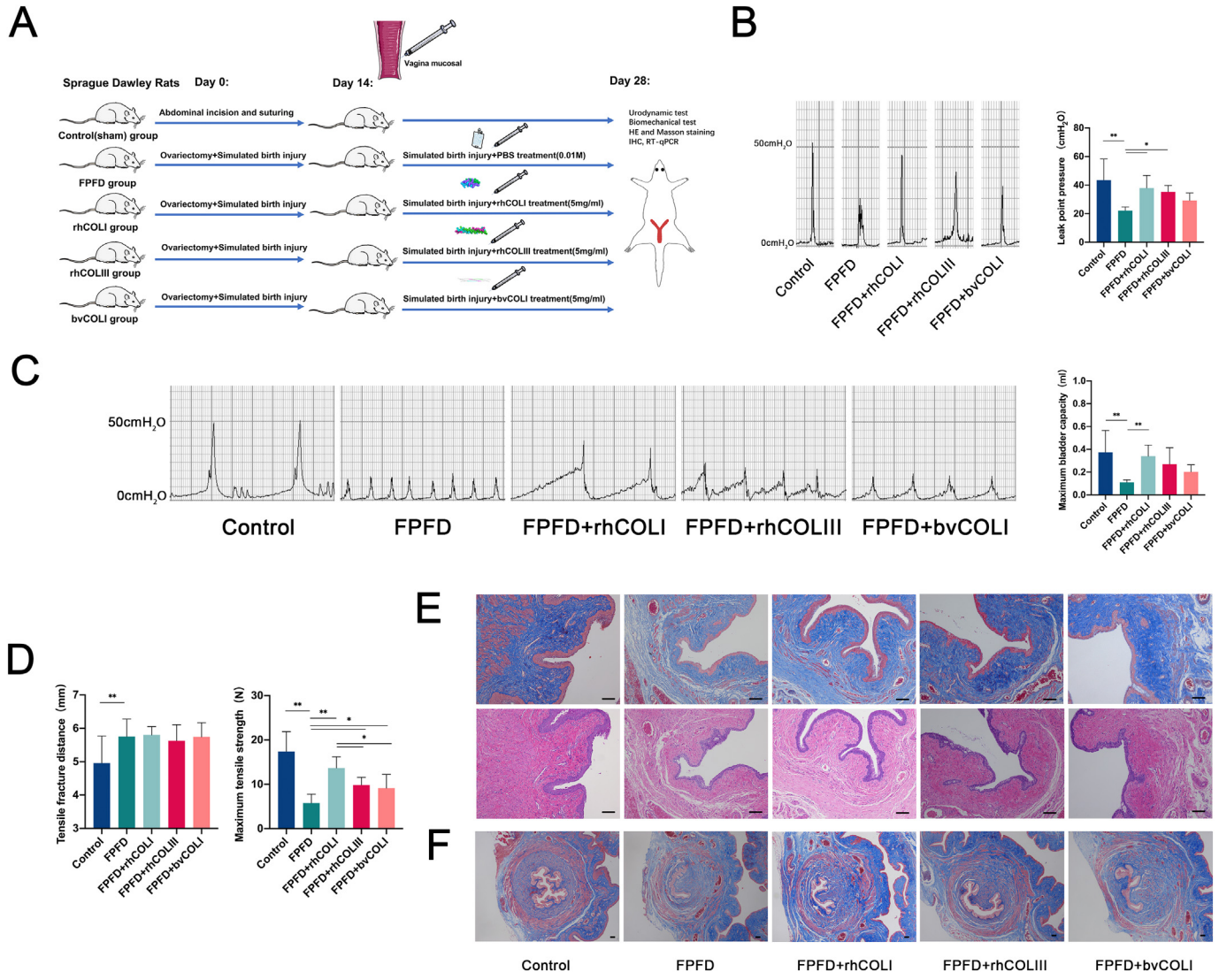

Fig. 6. rhCOL improved the histological features of FPFD rats. (A) Graphical flow of the animal experiments. (B) Maximum bladder capacity of rats in each group. (C) LPP obtained by urodynamic evaluations in each group. (D) Tensile fracture distance and maximum tensile strength obtained by biomechanical analysis in each group. (E) Masson's staining and H&E staining of the vagina in each group. (F) Masson's staining for the urethra in each group (scale bar = 100 μm) (*$P < 0.05$, **$P < 0.01$).

FPFD group, there was no significant difference. Comparing the biomechanical properties of the control group and FPFD group revealed significantly inferior results in the latter group, with a 67% decrease in the maximum tensile strength (Fig. 6D). After treatment with rhCOL and bvCOLI, the vaginal tensile capacity of rats was significantly enhanced compared to that of the FPFD group, and the recovery effect was more pronounced in rats treated with rhCOLI. In contrast, the biomechanical performance results of rats treated with rhCOL III were similar to those of rats treated with bvCOLI.

According to the H&E staining results (Fig. 6E), the vaginal epithelial tissues of rats in the control group were covered by a thick layer of squamous epithelial cells. The connective tissue of the lamina propria in the control group was rich in blood vessels and muscles. In contrast, the rats in the FPFD group had a thinner vaginal epithelial layer and fewer blood vessels than the control group. The muscularis in the FPFD group exhibited atrophy. After rhCOL and bvCOLI treatment, the number of blood vessels in the vaginal mucosal layer and muscularis significantly increased compared with that in the model group. Nevertheless, the recovery was the best in the rhCOLI group. Later, we labelled rhCOL with biotin. rhCOL showed a diffuse distribution around the vagina and persisted in the mucosal layer and muscularis for at least Fourteen days (Fig. S2B, S2C). To better visualize the muscularis and collagen fibre distribution, we performed Masson staining on the sections, with blue representing collagen fibres and red representing smooth muscle (Fig. 6E). In the control group, the four layers of the vagina were well-delineated in the control rats, the mucosal layer was rich in collagen fibrils with a well-ordered arrangement of collagen fibrils, and the fibromuscular layer was visible with an orderly arrangement. However, in the FPFD group, the vagina showed a loss of structure, and the fibromuscular layer was disrupted. Meanwhile, the collagen fibril content was reduced, and the collagen fibrils were disorganized. After rhCOL and bvCOLI treatment, the vagina was more structured, and the muscularis was better organized than in the FPFD group. Among the treatment groups, the recovery was the best in the rhCOLI group. The rats in the rhCOLIII and bvCOLI groups had similar appearances.

To evaluate urethral sphincter regeneration, urethral specimens were stained by MT. After the FPFD model was established, Masson staining showed that the urethral smooth muscle near the vagina was absent in the FPFD group of rats, the surrounding tissue structure was disrupted, and the number of collagen fibres was reduced (Fig. 6F). After rhCOL treatment, the smooth muscle of the urethra adjacent to the vagina was significantly hyperplastic, and the surrounding connective tissue structure was improved with increased collagen fibre content (Fig. 6F).

3.7. rhCOL promoted collagen synthesis and activated the FAK/RhoA/ROCK signalling pathway in the vaginal mucosa of rats

The results of immunohistochemistry and RT-PCR showed that the expression of collagen I and III was significantly reduced in the FPFD group compared with the control group, while the expression of the collagenase MMP2 increased and the expression of TIMP1 decreased (Fig. 7A). These

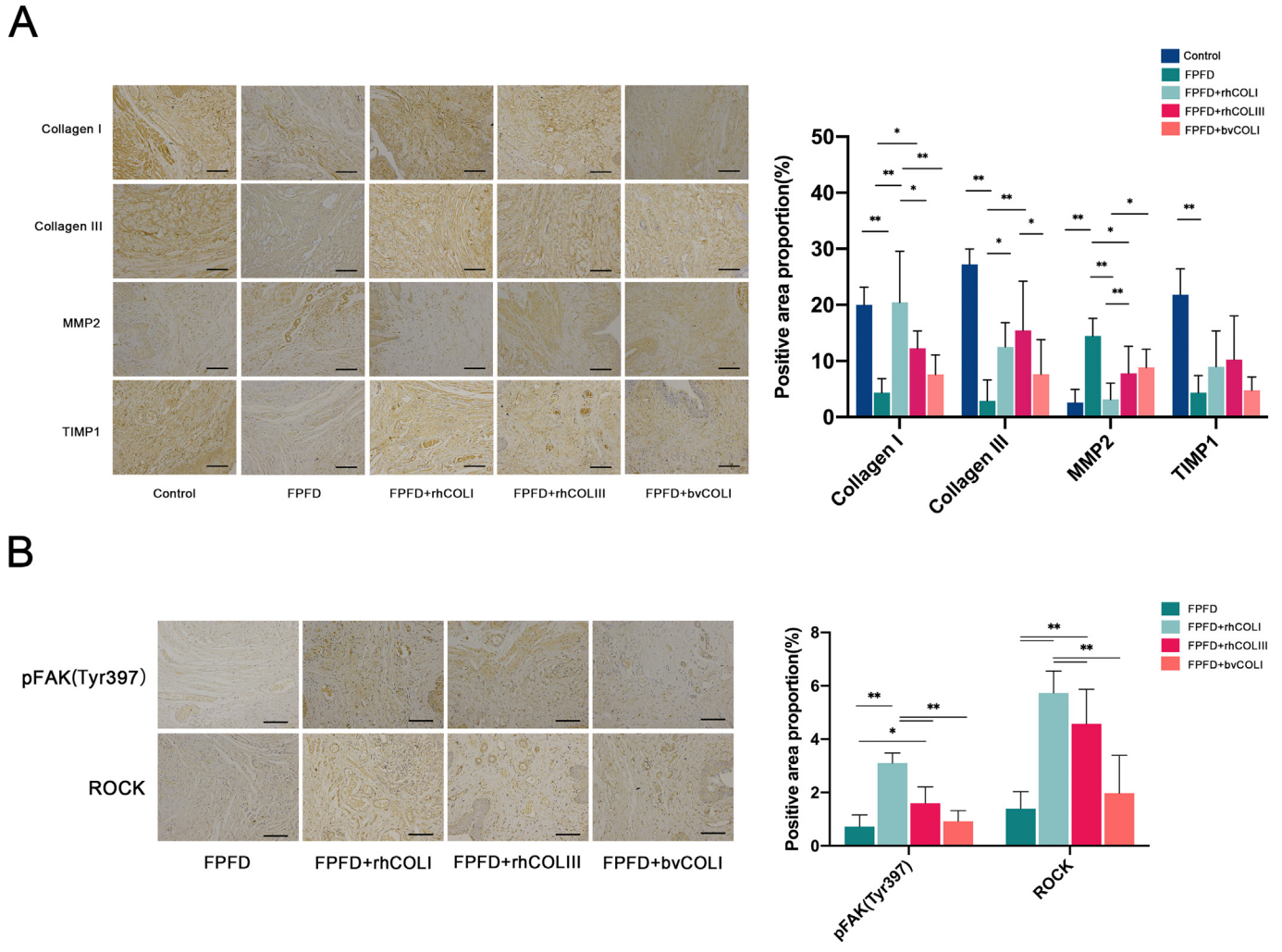

Fig. 7. rhCOL promoted collagen synthesis and activated the FAK/RhoA/ROCK signalling pathway in the rat vagina after 14 days of treatment. (A) Immunohistochemical staining of collagen I, collagen III, MMP2, and TIMP1 in the vaginal tissue of rats. (B) Immunohistochemical staining of pFAK (Tyr397) and ROCK in the vaginal tissue of rats (scale bar = 100 μm) (*$P < 0.05$, **$P < 0.01$).

findings indicated that FPFD rats developed apparent abnormalities in ECM metabolism and remodelling and that the metabolism of collagen protein exceeded the synthesis of collagen. After rhCOL treatment, the expression of collagen I and III was significantly increased, and the expression of MMP2 was decreased compared with that in the FPFD group. rhCOLI also promoted the expression of TIMP1 at the mRNA level (Fig. S2D). Overall, rhCOL treatment promoted collagen synthesis and inhibited collagen degradation, and rhCOLI had a more pronounced effect on collagen I synthesis and collagen metabolism than rhCOLIII. The treatment effect of bvCOLI was not significantly different compared with the FPFD group. To further confirm that collagen exerts biological effects through the activation of the FAK/RhoA/ROCK signalling pathway *in vivo*, we performed immunohistochemistry on rat vaginas. The results showed that rhCOL significantly promoted the expression of pFAK (Tyr397) and ROCK compared to that in the FPFD group (Fig. 7B).

4. Discussion

Multiple births and ageing are both contributing factors to the development of pelvic floor dysfunction. Childbirth is accompanied by excessive stretching and dilatation of the pelvic floor support structures, resulting in acute mechanical injury, which is the most significant risk factor for developing pelvic floor dysfunction later in life [35]. Ageing and oestrogen withdrawal can cause degenerative changes in the supporting structures of the pelvic floor, which in turn leads to a decrease in the mechanical resistance of the pelvic floor muscles, ligaments, fascia, and other connective tissues [36]. Therefore, we removed the bilateral ovaries of rats to simulate the ageing and low oestrogen level characteristics of FPFD patients and simulated the birth injury of FPFD patients by repeated vaginal dilatation and prolonged stretching. In our study, 14 days after modelling, the LPP and MBV of the model rats were significantly reduced, and the maximum mechanical stretch strength decreased, demonstrating the functional impairment of urodynamics and biomechanical damage of the vagina among the major organs of the rat pelvic floor. These injury-related changes were consistent with the clinical features of FPFD.

We attempted to demonstrate the excellent efficacy of rhCOL treating FPFD in the rat model. In our study, FPFD rats were treated with rhCOL, the expression of collagen I and III increased, MMP2 expression was inhibited, and TIMP1 expression increased, demonstrating that rhCOL adjusted the balance of ECM metabolism and remodelling. We also observed similar changes in the expression of collagen I and III *in vitro*. On the other hand, structural and functional alterations in FPFD rats allowed for a more effective assessment of collagen efficacy. The lamina propria and the muscularis are the main structures where the vagina and the urethra exchange substances and perform their functions [37], so this is the main reason why we chose the lamina propria and the muscularis as the site for rhCOL injection. rhCOL improved the urodynamic and biomechanical functions of FPFD rats, improved the arrangement of myogenic fibres and collagen structures in the lamina propria and muscle layer, increased collagen fibre content, and repaired damaged muscle layers. These results suggest that rhCOL may have promising efficacy in the treatment of FPFD.

The extracellular matrix of the pelvic floor tissue (vagina, ligaments) is composed mainly of fibroblasts and a small number of myofibroblasts, which are the main producers of collagen and necessary cells for connective tissue formation. Fibroblasts isolated from the sacral ligaments or vagina of patients with FPFD show the same reduced mechanical properties and impaired collagen metabolism as patients with FPFD [38–40]. Therefore, many articles related to FPFD have used HULFs as key cells for *in vitro* experiments [12,41,42]. Thus, we isolated fibroblasts from the uterosacral ligament of FPFD patients successfully *in vitro* to further investigate the biological effects of rhCOL on fibroblasts. We previously reported that rhCOLIII had a strong adhesive effect on the vaginal epithelium, which was associated with promoting recovery from vaginal atrophy. Potent cell adhesion might be helpful for promoting the viability of vaginal fibroblasts and smooth muscle cells, and it may strengthen the interaction between cells and the ECM to regulate biological function [25]. Our results show that rhCOLI had a strong ability to promote cell adhesion, which was 2.3-fold higher than that of the control group, while the ability of rhCOLIII was 1.3-fold and that of bvCOLI was 1.2-fold higher than that of the control group. Cell adhesive interactions were formed during the initial spreading, which primes cell functions and final fate determination [43]. We observed an increase in cell adhesion after recombinant collagen treatment accompanied by an increase in the cell-spreading area and observed cytoskeletal rearrangements. This morphological change has been observed by many researchers in recent years [44]. When collagen is recognized by cell membrane surface receptors, adhesion sites rapidly assemble to form focal adhesions, which act as local mechanoreceptors that transmit biomechanical signals from the local adhesion of the ECM to the cell, forming the entire cytoskeleton [45]. FAK plays a hub role in focal adhesion formation, which is reciprocally regulated by the ECM and cells or biomaterials through the phosphorylation of FAK [46]. Activated integrin β1 provides mechanical forces for the polymerization and organization of actin filaments, and biochemical signalling that modulate the formation of the adhesion complex triggers the autophosphorylation of FAK [47]. As expected, in our study, Vinculin expression levels and the phosphorylation of FAK in HULFs coincided with a trend of increased adhesion and collagen expression after treatment with rhCOL. Compared with other phosphorylation sites, pFAK (Tyr397) was most prominently expressed. Meanwhile, pFAK (Tyr397) and vinculin directly interacted, which is consistent with previous studies. In contrast, a pFAK397 inhibitor (PF573228) limited cell-spreading and collagen expression in rhCOL medium, and we also observed decreased vinculin expression. These results suggest that rhCOL enhances HULF adhesion and collagen expression by promoting FAK phosphorylation and focal adhesion formation.

The Rho family GTPases RhoA and Rho-associated kinases are key players in actin cytoskeleton regulation and cell adhesion. The Rho/ROCK signalling pathway activates downstream ROCK through Rho binding to GTP and further phosphorylates ROCK downstream substrates to remodel the cytoskeleton, induce actin-myosin contraction, and regulate microtubule dynamics [48]. *Sadia Afrin* et al. reported that pFAK (Tyr397) activates the RhoA/ROCK1 mechanotransduction pathways in human leiomyoma cells, leading to increased expression of collagen I [47]. *Jonghwa Kim* et al. found that both FAK and RhoA activation were associated with ECM remodelling in the liver [49]. In our study, we found that after treatment with rhCOL, the expression of RhoA-GTP and ROCK in HULFs was significantly upregulated. Both RhoA-GTP and ROCK were downregulated when an inhibitor of pFAK (Tyr397) (PF573228) and RhoA-GTP (C3 transferase) were added, respectively. In addition, a pFAK (Tyr397) inhibitor (PF573228) and a RhoA-GTP inhibitor (C3 transferase) had similar effects in reducing cell adhesion, migration and collagen synthesis. Furthermore, the pFAK(Tyr397) and RhoA-GTP expression were significantly increased in the rhCOLI group compared with the bvCOLI group, and there was also a trend of elevation in the rhCOLIII group. Therefore, we demonstrated that the underlying mechanism that rhCOL is superior to bvCOL is the higher activation level of the FAK/RhoA/ROCK pathway. The activation level of the rhCOLIII group was not significantly different from that of bvCOLI, probably due to the limitation of sample size.

Increased collagen synthesis and tissue structure restoration involve cellular metabolic processes, such as altered amino acid metabolism, increased cellular energy supply [50], and reduced oxidative damage [51]. Researchers found that collagen promoted the proline metabolic synthesis pathway [52] and reduced the level of ROS in damaged tissues [53]. However, the changes in metabolic processes associated with collagen supplementation have not yet been studied. Proline is an important constituent amino acid of collagen with key roles in protein structure, function, and the maintenance of cellular redox homeostasis. The present study results revealed that proline was significantly increased and that the arginine and proline metabolism pathways were upregulated in the rhCOLI and rhCOLIII groups. The increase in proline possibly promoted collagen synthesis by upregulating arginine and proline metabolism. The valine, leucine and isoleucine biosynthesis pathways were also upregulated in the rhCOLI and rhCOLIII groups. Valine, leucine and isoleucine are BCAAs that are traditionally associated with muscle growth and maintenance, energy

production, and the generation of neurotransmitter and gluconeogenic precursors [54], so the increase in BCAAs might be one of the important reasons for the repair of the muscularis of the vagina and urethra in rats. Glutathione is an antioxidant that plays a role in reducing oxidative stress, inhibiting apoptosis, and eliminating inflammatory responses [55]. rhCOLI promoted glutathione secretion, which provided a favourable growth environment for HULFs.

One limitation that may have affected this study was that we did not investigate the specific collagen recognition receptors. rhCOL has an important triple-helical sequence and a stable triple-helical structure, which are potential recognition targets for the collagen recognition receptor integrins as well as the DNA-damage response (DDR). Current studies have shown that integrins and the DDR play an essential role in dynamic connective tissue remodelling and may contribute to tissue structure remodelling and restoration [56]. Furthermore, cell-ECM adhesions mainly involve integrins. At the adhesion site, integrin binds its ECM ligands and initiates intracellular signalling [57]. Direct cellular targets might need to be studied in-depth to clarify the mechanism involved. Second, due to financial and workload constraints, we selected only one experimental observation time point based on preliminary experimental results.

5. Conclusion

In conclusion, rhCOL prevents adverse pelvic floor tissue remodelling and improves pelvic floor function in a model of pelvic floor dysfunction in rats, possibly by promoting cell adhesion, migration, and ECM synthesis by activating the FAK/RhoA/ROCK signalling pathway. Meanwhile, compared to rhCOLIII, rhCOLI appears to be more effective for the repair of pelvic floor musculature and connective tissue, promotion of cell adhesion, expression of collagen I, and regulation of cellular metabolism. These findings suggest that the perivaginal injection of rhCOL is a very promising treatment method for FPFD that may be used in the future in the clinic.

CRediT authorship contribution statement

Hu Li: Conceptualization, Methodology, Software, Investigation, Writing - Original Draft.

Shuang You: Visualization, Methodology, Software.

Xia Yang: Resources, Editing, Consulting.

Shuaibin Liu: Methodology, Writing - Review & Editing, Formal Analysis, Supervision.

Lina Hu: Resources, Writing - Review & Editing, Supervision, Data Curation.

Data availability statement

The raw/processed data required to reproduce these findings cannot be shared at this time as the data also forms part of an ongoing study. Anyone who are interested in this study can contact the corresponding authors to obtain more information.

Declaration of competing interest

There are no conflicts to declare.

Acknowledgements

This work was supported by the Chongqing Municipal Education Commission (KJCXZD2020017). We gratefully acknowledge Shanxi Jinbo Bio-Pharmaceutical CO., Ltd. for their help in providing rhCOLI and rhCOLIII, as designed.

Appendix A. Supplementary data

Supplementary data to this article can be found online at https://doi.org/10.1016/j.msec.2022.112715.

References

[1] J.M. Wu, C.A. Matthews, M.M. Conover, V. Pate, M. Jonsson Funk, Lifetime risk of stress urinary incontinence or pelvic organ prolapse surgery, Obstet. Gynecol. 123 (6) (2014) 1201–1206.

[2] B. Megabiaw, M. Adefris, G. Rortveit, G. Degu, M. Muleta, A. Blystad, T. Kiserud, T. Melese, Y. Kebede, Pelvic floor disorders among women in Dabat district, northwest Ethiopia: a pilot study, Int. Urogynecol. J. 24 (7) (2013) 1135–1143.

[3] R.M. Islam, R.J. Bell, B. Billah, M.B. Hossain, S.R. Davis, The prevalence of symptomatic pelvic floor disorders in women in Bangladesh, Climacteric 19 (6) (2016) 558–564.

[4] L. Zhu, J. Lang, C. Liu, S. Han, J. Huang, X. Li, The epidemiological study of women with urinary incontinence and risk factors for stress urinary incontinence in China, Menopause 16 (4) (2009) 831–836.

[5] G. D'Alessandro, S. Palmieri, A. Cola, M. Barba, S. Manodoro, M. Frigerio, Detrusor underactivity prevalence and risk factors according to different definitions in women attending urogynecology clinic, Int. Urogynecol. J. (2021)https://doi.org/10.1007/s00192-021-04796-w In press.

[6] M.A.H. Hage-Fransen, M. Wiezer, A. Otto, M.S. Wieffer-Platvoet, M.H. Slotman, M.W.G. Nijhuis-van der Sanden, A.L. Pool-Goudzwaard, Pregnancy- and obstetric-related risk factors for urinary incontinence, fecal incontinence, or pelvic organ prolapse later in life: a systematic review and meta-analysis, Acta Obstet. Gynecol. Scand. 100 (3) (2021) 373–382.

[7] M.D. Barber, L. Brubaker, K.L. Burgio, H.E. Richter, I. Nygaard, A.C. Weidner, S.A. Menefee, E.S. Lukacz, P. Norton, J. Schaffer, J.N. Nguyen, D. Borello-France, P.S. Goode, S. Jakus-Waldman, C. Spino, L.K. Warren, M.G. Gantz, S.F. Meikle, N.Human Development Pelvic Floor Disorders</collab> <collab>H. Eunice Kennedy Shriver National Institute of Child, Comparison of 2 transvaginal surgical approaches and perioperative behavioral therapy for apical vaginal prolapse: the OPTIMAL randomized trial, JAMA 311 (10) (2014) 1023–1934.

[8] V. Kirchin, T. Page, P.E. Keegan, K.O. Atiemo, J.D. Cody, S. McClinton, P. Aluko, Urethral injection therapy for urinary incontinence in women, Cochrane Database Syst. Rev. 7 (2017), CD003881.

[9] X. Fritel, S. Campagne-Loiseau, M. Cosson, P. Ferry, C. Saussine, J.P. Lucot, D. Salet-Lizee, M.L. Barussaud, T. Boisrame, C. Carlier-Guerin, T. Charles, P. Debodinance, X. Deffieux, A.C. Pizzoferrato, S. Curinier, S. Ragot, V. Ringa, R. de Tayrac, A. Fauconnier, Complications after pelvic floor repair surgery (with and without mesh): short-term incidence after 1873 inclusions in the French VIGI-MESH registry, BJOG 127 (1) (2020) 88–97.

[10] B. Chen, J. Yeh, Alterations in connective tissue metabolism in stress incontinence and prolapse, J. Urol. 186 (5) (2011) 1768–1772.

[11] M. Budatha, S. Roshanravan, Q. Zheng, C. Weislander, S.L. Chapman, E.C. Davis, B. Starcher, R.A. Word, H. Yanagisawa, Extracellular matrix proteases contribute to progression of pelvic organ prolapse in mice and humans, J. Clin. Invest. 121 (5) (2011) 2048–2059.

[12] M. Vashaghian, C.M. Diedrich, B. Zandieh-Doulabi, A. Werner, T.H. Smit, J.P. Roovers, Gentle cyclic straining of human fibroblasts on electrospun scaffolds enhances their regenerative potential, Acta Biomater. 84 (2019) 159–168.

[13] K.A. Connell, M.K. Guess, H. Chen, V. Andikyan, R. Bercik, H.S. Taylor, HOXA11 is critical for development and maintenance of uterosacral ligaments and deficient in pelvic prolapse, J. Clin. Invest. 118 (3) (2008) 1050–1055.

[14] A.A. Ewies, F. Al-Azzawi, J. Thompson, Changes in extracellular matrix proteins in the cardinal ligaments of post-menopausal women with or without prolapse: a computerized immunohistomorphometric analysis, Hum. Reprod. 18 (10) (2003) 2189–2195.

[15] C. Goepel, L. Hefler, H.D. Methfessel, H. Koelbl, Periurethral connective tissue status of postmenopausal women with genital prolapse with and without stress incontinence, Acta Obstet. Gynecol. Scand. 82 (7) (2003) 659–664.

[16] H. Li, M. Bao, Y. Nie, Extracellular matrix-based biomaterials for cardiac regeneration and repair, Heart Fail. Rev. 26 (5) (2021) 1231–1248.

[17] X. Liu, Y. Gao, X. Long, T. Hayashi, K. Mizuno, S. Hattori, H. Fujisaki, T. Ogura, D.O. Wang, T. Ikejima, Type I collagen promotes the migration and myogenic differentiation of C2C12 myoblasts via the release of interleukin-6 mediated by FAK/NF-kappaB p65 activation, Food Funct. 11 (1) (2020) 328–338.

[18] C.G. Knight, L.F. Morton, A.R. Peachey, D.S. Tuckwell, R.W. Farndale, M.J. Barnes, The collagen-binding A-domains of integrins alpha(1)beta(1) and alpha(2)beta(1) recognize the same specific amino acid sequence, GFOGER, in native (triple-helical) collagens, J. Biol. Chem. 275 (1) (2000) 35–40.

[19] S. McLaughlin, B. McNeill, J. Podrebarac, K. Hosoyama, V. Sedlakova, G. Cron, D. Smyth, R. Seymour, K. Goel, W. Liang, K.J. Rayner, M. Ruel, E.J. Suuronen, E.I. Alarcon, Injectable human recombinant collagen matrices limit adverse remodeling and improve cardiac function after myocardial infarction, Nat. Commun. 10 (1) (2019) 4866.

[20] M. Dai, B. Sui, Y. Xue, X. Liu, J. Sun, Cartilage repair in degenerative osteoarthritis mediated by squid type II collagen via immunomodulating activation of M2 macrophages, inhibiting apoptosis and hypertrophy of chondrocytes, Biomaterials 180 (2018) 91–103.

[21] D. Zhang, X. Wu, J. Chen, K. Lin, The development of collagen based composite scaffolds for bone regeneration, Bioact. Mater. 3 (1) (2018) 129–138.

[22] Y. Xu, M. Kirchner, Collagen mimetic peptides, Bioengineering (Basel) 8 (1) (2021) 5.

[23] P. Fagerholm, N.S. Lagali, K. Merrett, W.B. Jackson, R. Munger, Y. Liu, J.W. Polarek, M. Soderqvist, M. Griffith, A biosynthetic alternative to human donor tissue for inducing corneal regeneration: 24-month follow-up of a phase 1 clinical study, Sci. Transl. Med. 2 (46) (2010), 46ra61.

[24] D. Konig, S. Oesser, S. Scharla, D. Zdzieblik, A. Gollhofer, Specific collagen peptides improve bone mineral density and bone markers in postmenopausal women-a randomized controlled study, Nutrients 10 (1) (2018) 97.

[25] S. You, S. Liu, X. Dong, H. Li, Y. Zhu, L. Hu, Intravaginal administration of human type III collagen-derived biomaterial with high cell-adhesion activity to treat vaginal atrophy in rats, ACS Biomater. Sci. Eng. 6 (4) (2020) 1977–1988.
[26] S.J. Hwang, S.H. Kim, W.Y. Seo, Y. Jeong, M.C. Shin, D. Ryu, S.B. Lee, Y.J. Choi, K. Kim, Effects of human collagen alpha-1 type I-derived proteins on collagen synthesis and elastin production in human dermal fibroblasts, BMB Rep. 54 (6) (2021) 329–334.
[27] S. Hong, H. Li, D. Wu, B. Li, C. Liu, W. Guo, J. Min, M. Hu, Y. Zhao, Q. Yang, Oxidative damage to human parametrial ligament fibroblasts induced by mechanical stress, Mol. Med. Rep. 12 (4) (2015) 5342–5348.
[28] K.F. Smart, R.B. Aggio, J.R. Van Houtte, S.G. Villas-Boas, Analytical platform for metabolome analysis of microbial cells using methyl chloroformate derivatization followed by gas chromatography-mass spectrometry, Nat. Protoc. 5 (10) (2010) 1709–1729.
[29] Y. Liu, T.L. Han, X. Luo, Y. Bai, X. Chen, W. Peng, X. Xiong, P.N. Baker, C. Tong, H. Qi, The metabolic role of LncZBTB39-1:2 in the trophoblast mobility of preeclampsia, Genes Dis. 5 (3) (2018) 235–244.
[30] Z. Pang, J. Chong, G. Zhou, D.A. de Lima Morais, L. Chang, M. Barrette, C. Gauthier, P.E. Jacques, S. Li, J. Xia, MetaboAnalyst 5.0: narrowing the gap between raw spectra and functional insights, Nucleic Acids Res. 49 (W1) (2021) W388–W396.
[31] B. Zhao, Q. Sun, Y. Fan, X. Hu, L. Li, J. Wang, S. Cui, Transplantation of bone marrow-derived mesenchymal stem cells with silencing of microRNA-138 relieves pelvic organ prolapse through the FBLN5/IL-1beta/elastin pathway, Aging (Albany NY) 13 (2) (2021) 3045–3059.
[32] C. Hua, Y. Zhu, W. Xu, S. Ye, R. Zhang, L. Lu, S. Jiang, Characterization by high-resolution crystal structure analysis of a triple-helix region of human collagen type III with potent cell adhesion activity, Biochem. Biophys. Res. Commun. 508 (4) (2019) 1018–1023.
[33] P. Banerjee, G. Suseela, C. Shanthi, Isolation and identification of cryptic bioactive regions in bovine achilles tendon collagen, Protein J. 31 (5) (2012) 374–386.
[34] B. Cheng, W. Wan, G. Huang, Y. Li, G.M. Genin, M.R.K. Mofrad, T.J. Lu, F. Xu, M. Lin, Nanoscale integrin cluster dynamics controls cellular mechanosensing via FAKY397 phosphorylation, Sci. Adv. 6 (10) (2020), eaax1909.
[35] M. Alperin, A. Feola, L. Meyn, R. Duerr, S. Abramowitch, P. Moalli, Collagen scaffold: a treatment for simulated maternal birth injury in the rat model, Am. J. Obstet. Gynecol. 202 (6) (2010) 589 e1-e8.
[36] P.A. Moalli, K.M. Debes, L.A. Meyn, N.S. Howden, S.D. Abramowitch, Hormones restore biomechanical properties of the vagina and supportive tissues after surgical menopause in young rats, Am. J. Obstet. Gynecol. 199 (2) (2008) 161 e1-e8.
[37] L. Berger, M. El-Alfy, C. Martel, F. Labrie, Effects of dehydroepiandrosterone, premarin and acolbifene on histomorphology and sex steroid receptors in the rat vagina, J. Steroid Biochem. Mol. Biol. 96 (2) (2005) 201–215.
[38] A.M. Ruiz-Zapata, M.H. Kerkhof, B. Zandieh-Doulabi, H.A. Brolmann, T.H. Smit, M.N. Helder, Fibroblasts from women with pelvic organ prolapse show differential mechanoresponses depending on surface substrates, Int. Urogynecol. J. 24 (9) (2013) 1567–1575.
[39] A.M. Ruiz-Zapata, M.H. Kerkhof, B. Zandieh-Doulabi, H.A. Brolmann, T.H. Smit, M.N. Helder, Functional characteristics of vaginal fibroblastic cells from premenopausal women with pelvic organ prolapse, Mol. Hum. Reprod. 20 (11) (2014) 1135–1143.
[40] H. Kufaishi, M. Alarab, H. Drutz, S. Lye, O. Shynlova, Comparative characterization of vaginal cells derived from premenopausal women with and without severe pelvic organ prolapse, Reprod. Sci. 23 (7) (2016) 931–943.
[41] I. Han, S.A. Choi, S.I. Kim, E.H. Choi, Y.J. Lee, Y. Kim, Improvement of cell growth of uterosacral ligament fibroblast derived from pelvic organ prolapse patients by cold atmospheric plasma treated liquid, Cells 10 (10) (2021).
[42] M. Qin, J. Jin, Q. Saiding, Y. Xiang, Y. Wang, F. Sousa, B. Sarmento, W. Cui, X. Chen, In situ inflammatory-regulated drug-loaded hydrogels for promoting pelvic floor repair, J. Control. Release 322 (2020) 375–389.
[43] S.M.C. Bruekers, M. Bao, J.M.A. Hendriks, K.W. Mulder, W.T.S. Huck, Adaptation trajectories during adhesion and spreading affect future cell states, Sci. Rep. 7 (1) (2017) 12308.
[44] L. Yu, Y. Hou, W. Xie, J.L. Cuellar-Camacho, Q. Wei, R. Haag, Self-strengthening adhesive force promotes cell mechanotransduction, Adv. Mater. 32 (52) (2020), e2006986.
[45] M.A. Nosenko, A.M. Moysenovich, A.Y. Arkhipova, K.N. Atretkhany, S.A. Nedospasov, M.S. Drutskaya, M.M. Moisenovich, Fibroblasts upregulate expression of adhesion molecules and promote lymphocyte retention in 3D fibroin/gelatin scaffolds, Bioact. Mater. 6 (10) (2021) 3449–3460.
[46] C.C. Lin, S.J. Fu, Osteogenesis of human adipose-derived stem cells on poly(dopamine)-coated electrospun poly(lactic acid) fiber mats, Mater. Sci. Eng. C Mater. Biol. Appl. 58 (2016) 254–263.
[47] S. Afrin, M.S. Islam, K. Patzkowsky, M. Malik, W.H. Catherino, J.H. Segars, M.A. Borahay, Simvastatin ameliorates altered mechanotransduction in uterine leiomyoma cells, Am. J. Obstet. Gynecol. 223 (5) (2020) 733.e1–733.e14.
[48] R. Zhang, T.A. Elkhooly, Q. Huang, X. Liu, X. Yang, H. Yan, Z. Xiong, J. Ma, Q. Feng, Z. Shen, A dual-layer macro/mesoporous structured TiO2 surface improves the initial adhesion of osteoblast-like cells, Mater. Sci. Eng. C Mater. Biol. Appl. 78 (2017) 443–451.
[49] J. Kim, W. Kang, S.H. Kang, S.H. Park, J.Y. Kim, S. Yang, S.Y. Ha, Y.H. Paik, Proline-rich tyrosine kinase 2 mediates transforming growth factor-beta-induced hepatic stellate cell activation and liver fibrosis, Sci. Rep. 10 (1) (2020) 21018.
[50] R.B. Hamanaka, G.M. Mutlu, The role of metabolic reprogramming and de novo amino acid synthesis in collagen protein production by myofibroblasts: implications for organ fibrosis and cancer, Amino Acids 53 (2021) 1851–1862.
[51] H. Saito-Takatsuji, Y. Yoshitomi, Y. Ishigaki, S. Yamamoto, N. Numata, Y. Sakai, M. Takeuchi, N. Tomosugi, S. Katsuda, H. Yonekura, T. Ikeda, Protective effects of collagen tripeptides in human aortic endothelial cells by restoring ROS-induced transcriptional repression, Nutrients 13 (7) (2021) 2226.
[52] M. Fruchtl, J. Sakon, R. Beitle, Expression of a collagen-binding domain fusion protein: effect of amino acid supplementation, inducer type, and culture conditions, Biotechnol. Prog. 31 (2) (2015) 503–509.
[53] M. Pozzolini, E. Millo, C. Oliveri, S. Mirata, A. Salis, G. Damonte, M. Arkel, S. Scarfi, Elicited ROS scavenging activity, photoprotective, and wound-healing properties of collagen-derived peptides from the marine sponge Chondrosia reniformis, Mar. Drugs 16 (12) (2018) 465.
[54] A. Kitsy, S. Carney, J.C. Vivar, M.S. Knight, M.A. Pointer, J.K. Gwathmey, S. Ghosh, Effects of leucine supplementation and serum withdrawal on branched-chain amino acid pathway gene and protein expression in mouse adipocytes, PLoS One 9 (7) (2014), e102615.
[55] F. Silvagno, A. Vernone, G.P. Pescarmona, The role of glutathione in protecting against the severe inflammatory response triggered by COVID-19, Antioxidants (Basel) 9 (7) (2020) 624.
[56] H. Xu, D. Bihan, F. Chang, P.H. Huang, R.W. Farndale, B. Leitinger, Discoidin domain receptors promote alpha1beta1- and alpha2beta1-integrin mediated cell adhesion to collagen by enhancing integrin activation, PLoS One 7 (12) (2012), e52209.
[57] B.D. Hoffman, C. Grashoff, M.A. Schwartz, Dynamic molecular processes mediate cellular mechanotransduction, Nature 475 (7356) (2011) 316–323.